Bayesian Inference of Collision Avoidance Intent during Ship Encounters

Chengfeng Jia, Jie Ma*, Bert de Vries, Wouter M. Kouw

Abstract—Ship collision accidents frequently cause casualties and significant property losses. These collisions mainly occur by incorrectly interpreting the intents of other ships' navigators. However, inferring the avoidance intents of other ships is challenging, because the uncertain motions and the long-lasting dynamic interactions during encounters usually obscure the true intents. To address this, we propose a probabilistic graph model to infer the hidden avoidance intent of ships. Specifically, the dynamic encounter evolution is expressed in a model represented by a factor graph, where the intent beliefs are accumulated and propagated over time through message passing in the graph. In the inference procedure, we develop a hybrid Bayesian inference approach, integrating a data-driven component derived from empirical priors fitted to historical data, and a model-driven component capturing the ship's control process. We derive 9 types of intents from naturalistic ship encounters and evaluate the model on a validation split. The quantitative metrics demonstrate that, on average, the proposed procedure can accurately infer the intents 14.04 seconds in advance and outperforms the baseline in macro-averaged recall rate (0.2919) and F1-score (0.2843).

Note to Practitioners— This work aims to enhance safety in ship navigation by introducing an intelligent navigation support system to prevent collisions. A significant cause of ship collision accidents is the misinterpretation of other navigators' intents. Estimating the intents of marine traffic participants can significantly reduce collision rates. However, real-time intent inference in ship encounters poses challenges due to complex dynamics and uncertain motions. We propose a novel probabilistic graphical model that allows us to infer avoidance intents, evaluated on a naturalistic Automatic Identification System (AIS) dataset, demonstrating effectiveness in real-world scenarios. The practical implications of our work are substantial for the maritime industry. Ship captains and intelligent automated vessels can use our system to enhance situational awareness, enabling informed collision avoidance decisions. Our work aims to improve the safety and efficiency of ship navigation, reducing collision risks and ensuring the well-being of crew members and valuable cargo.

Index Terms—Intent inference, Bayesian inference, factor graph, collision risk, navigational safety, intelligent ship.

Chengfeng Jia is affiliated with State Key Laboratory of Maritime Technology and Safety, and School of Navigation, Wuhan University of Technology, Wuhan 430063, China, and Department of Electrical Engineering, TU Eindhoven, Eindhoven 5600MB, the Netherlands (c.jia@tue.nl).

Jie Ma is affiliated with State Key Laboratory of Maritime Technology and Safety, and School of Navigation, Wuhan University of Technology, Wuhan 430063, China (majie@whut.edu.cn)

Bert de Vries (a.de.vries@tue.nl) and Wouter M. Kouw (w.m.kouw@tue.nl) are affiliated with Department of Electrical Engineering, TU Eindhoven, Eindhoven 5600MB, the Netherlands.

I. INTRODUCTION

Maritime transport is immensely important to global trade, but collisions remain a threat to marine traffic and the environment [1]. The collision statistics reported by the China Maritime Safety Administration (MSA), indicate that 41.17% of collision accidents were caused by hazardous encounter situations [2]. During encounters, ship officers must decide how to avoid others based on the perceived intent of the other ship. But many ship-to-ship conflicts and collisions are caused by officers' inability to correctly identify others' intents. This issue is exemplified in the official report [3] detailing the collision between Jiahe 128 and Guiqinyu 22668, wherein a misjudgment of avoidance intents resulted in an erroneous navigational decision during the encounter, culminating in a collision. The timely and effective identification of avoidance intents in the encounter situation affords the officers a greater temporal and spatial allowance for making informed decisions, consequently mitigating the collision risk.

The International Maritime Organization (IMO) adopted the Convention on the International Regulations for Preventing Collisions at Sea (COLREGs) [4], which provides guidelines on which ship has priority to avoid and how evasive procedures should be taken. However, not all ships strictly adhere to the COLREGs [5]. Furthermore, the inherent flexibility in rule interpretation leads to variation in what actions are taken by encountering ships. For instance, an overtaking ship is allowed to pass by both the port and starboard side of another ship. Rather than strict observance of the COLREGs, the ship officers decide how to avoid dangerous encounter situations, that is the intent. Note that ship encounters are long-lasting processes. The relative motions between pairs of ships will continuously change as the situation unfolds [6]. Therefore, the intent to avoid is not formed abruptly, but rather evolves and grows as the encounter develops. Ship officers gradually become more convinced of the intent through continuous observation of other ships. This highlights the need to model the dynamic encounter process instead of instantaneous motions to identify intent. However, formulating how intent beliefs evolve and detecting hidden intents over time present significant challenges.

Although intent inference is a popular area of research in road and air transportation [7], [8], [9], research on intent inference for maritime ships is scarce. Deep learning-based methods are currently the best performing methods for driving intent and flight intent inference. These methods learn the implicit relationship between motions and intent from massive historical data sets. However, the availability of massive data

sets for marine traffic is limited due to the high costs associated with data collection and label calibration. Furthermore, compared to land vehicles and aircraft, ships operate in an environment that lacks fixed lanes and sophisticated controllers to constrain their motions. This leads to a higher degree of uncertainty in ship encounters. Ships exhibit complex and diverse motion patterns that cannot be adequately captured solely through historical data [10]. Additionally, ship captains hold the responsibility of deciding whether to initiate specific evasive procedures. However, even with the same avoidance intent, the actions taken by captains can vary significantly due to factors such as their personal operational expertise, prevailing environmental conditions, and the dynamic interactions between ships. The presence of these influential factors further compounds the challenge of accurately inferring avoidance intents in encounter situations.

We choose a probabilistic framework to tackle the inherent uncertainty in the encounter process and the inherent complexity of collision avoidance intents. In this framework, we model the ship encounter as a stochastic process that characterizes the uncertainties using probability distributions. The accumulation of intents may then be inferred by means of a message passing procedure on a factor graph, combining predictions based on dynamics with information from observations. Our specific contributions are outlined below:

- To capture how encounter situations evolve over time, we propose a dynamic probabilistic graphical model applied recursively over time. The model is expressed in terms of a Forney-style factor graph which explicitly tracks uncertainty across low-level operations, thereby ensuring explainability of estimates and subsequent decisions. The recursive nature of the model means inferred intents are updated for each new observation, which aligns with the natural mechanism of intent accumulation by navigators during ship encounters.
- For the inference procedure, we develop a hybrid approach. The model-driven component represents the intent-related ship physical dynamics as a stochastic process, modeling the transmission of motion states under the intended control policy. The data-driven component fits an empirical prior to capture the control patterns exhibited by different captains in historical data, providing valuable insights into their collision avoidance process.
- With the limited training data available, the proposed inference model performs better than existing deep learning models. The experimental results show 9 types of avoidance intent that can be inferred in advance.

II. RELATED WORK

Recently, researchers have been focusing on developing collision-avoidance navigation systems for enhancing navigation safety. Especially for ship encounters, several collision risk indicators (CRI) are proposed to assess degrees of danger. Among these indicators, distance to the closest point of approach (DCPA) and time to the closest point of approach (TCPA) are the most widely used [11]. Zhao et al. [12] consider the ship dimension and adopted a polygon

to represent the ship position, based on AIS data to correct DCPA and TCPA. However, most collision risk indicators assume that ships will keep their speed and heading. In fact, during encounters, the ship officers need to decide future maneuvering based on the development of the ships involved [13]. Especially in busy areas, such as intersection waterways, the ship changes motion states more frequently to avoid potential collisions. If the avoidance intent can be inferred in advance, there will be more time to react and ensure safe and efficient navigation.

Although the COLREGs define collision avoidance for encountering ship pairs, in many cases, ships do not strictly comply with the rules. To this end, Cho et al. [14] interpret avoidance intent as the probability of complying with the COLREGs and propose a dynamic Bayesian network to infer the intents. Later, Cho et al. [15] combine the intent inference results with a new probabilistic Velocity Obstacle algorithm to develop a collision avoidance approach involving COLREG-violating ships. However, these avoidance intents are limited to the two categories, which are compliance or violation of the COLREGs. Wang et al. [16] proposed a collision avoidance scheme, in which intentions to "give way" or "stand on" are inferred based on the Dempster-Shafer belief functions. The limitation of this work is that the evidence discrepancy threshold parameter is hard to determine. Moreover, these above methods were only verified in the simulations. Wang et al. [17] developed an adaptive intent inference model based on fuzzy system design. The main components, the membership function and the prior, of a fuzzy system, are tricky to design and highly rely on expert experience. Du et al. [18] proposed an intention estimation method for the "give-way" ship. The turning points were detected by a Douglas-Peucker algorithm and thorough risk analysis to determine the intents. However, turning points can be only detected when the ship has been maneuvering for at least some time. The delayed inferred intent results will hinder the application for collision avoidance.

Learning-based methods are state-of-the-art for intent inference in land and air transportation modeling. Intent inference is usually treated as a classification task. Many machine learning models, such as the support vector machine (SVM) [7], random forest (RF) [19], long short-term memory network (LSTM) [20], ensemble LSTM (ELSTM) [9] have been developed to relate motion features to hidden intent classes. These algorithms require a large amount of data for training models that contain a large number of parameters. However, there is no open source data or benchmark for ship trajectory to support training of these models. Therefore, models with a large number of parameters are rarely deployed in practical settings.

Alternatively, Bayesian modeling has recently drawn quite some attention in the machine learning community for its data efficiency and fundamental treatment of uncertainty [21]. Bayesian models has been successfully adopted in many applications such as deteriorating system monitoring [22], processing of incomplete industrial data sets [23], perception and location modeling [24], as well as path planing [25]. A factor graph represents a (network-based) visualization of

statistical independencies between the factors in a probabilistic model. In a Forney-style Factor Graph (FFG), edges are associated with variables in the model and nodes represent statistical constraints between connected variables [26]. FFGs provide a convenient mathematical framework for dynamical models, where sets of factors recur over time. Bayesian inference can be formalized as a process of message passing between nodes, where a message towards an edge represents the information gathered by the node across all its other edges [27]. This reduces the needed computations to local function evaluations, thus forming an efficient distributed inference algorithm. Examples of Bayesian inference on factor graphs include environment resolution [28], path planning for multi-agent [29], targets tracking [30] and audio processing [31].

In summary, the existing methods for intent inference in ship navigation lack validation with realistic data or the capability to infer intent in real-time, thereby hindering their application in the real world. While intent inference in road and air traffic is inspiring, challenges stemming from limited datasets and uncertain encounter process make direct application to intention inference difficult. Therefore, this work model the ship encounter as a stochastic process, and intents are inferred by the message passing procedure on a factor graph. To the best of our knowledge, this study is the first to explore the use of message passing method for intent inference in ship navigation.

III. PROBLEM STATEMENT

Ship pairs may try to avoid collisions during encounters in different ways. We study encountering situations between two ships that are referred to, for simplicity's sake, as *own ship* and *target ship*. Our work aims to infer, from the own ship's perspective, the avoidance intent of the target ship. The avoidance intent at time step t, denoted by I_t, consists of various combinations of acceleration levels and turning rates. We have categorized these into a set $\mathbb{I}$ as follows:

$$\mathbb{I} = \begin{cases} i_1 & \text{if turn left and accelerate} \\ i_2 & \text{if keep straight and accelerate} \\ i_3 & \text{if turn right and accelerate} \\ i_4 & \text{if turn left and keep speed} \\ i_5 & \text{if keep straight and keep speed} \\ i_6 & \text{if turn right and keep speed} \\ i_7 & \text{if turn left and decelerate} \\ i_8 & \text{if keep straight and decelerate} \\ i_9 & \text{if turn right and decelerate} \,. \end{cases} \quad (1)$$

In Fig. 1, the own ship (O) encounters a target ship (T), and the target ship has various ways to react.

In practice, the officers of the own ship use the AIS data of the target ship to estimate the intents of its officers. However, these data lack explicit intent or control information and often include substantial noise in location and speed. This paper aims to infer the hidden intents from the noisy time series, a problem known as filtering. From the perspective of Bayesian inference, our goal is to calculate the posterior probability

$p(I_t \mid z_{1:t})$ of intent from the observation sequence $z_{1:t}$ from AIS data.

IV. MODEL SPECIFICATION

We propose a Bayesian inference approach to estimate avoidance intent. Firstly, we specify an intent-driven dynamical model for the ship. Then, we cast this model to a factor graph representation and apply automatable message passing-based recursive Bayesian inference on that graph.

A. Full probabilistic model

To formulate the encounter process, we design a probabilistic dynamical model, that is written as the joint distribution of intents, controls, states, and observations

$$p(z, s, I, u) =$$
$$p(s_0) \prod_{t=1}^{T} p(z_t \mid s_t) \, p(s_t \mid s_{t-1}, u_t) \, p(u_t \mid I_t) \, p(I_t), \quad (2)$$

where z_t denotes the observation, s_t denotes the motion state of the ship, u_t denotes the control signal, I_t denotes the intent. The variables without subscript refer to the entire time series, e.g., $z = z_{1:T}$. The joint distribution of intents, controls, states, and observations reveals the conditional relationship between these variables during the encountering process. In the following, we will explain the details of each probability.

B. Likelihood of observations

For inferring the intent of the target ship, the COLREGs require every ship to maintain a proper look-out. The AIS data set provides a massive amount of information to support the encounter situation awareness and intent inference. Through observation and calculation, we can obtain the relative motion parameters of two ships

$$z_t = \begin{bmatrix} \Delta x_t & \Delta y_t & \Delta \phi_t & \Delta v_t \end{bmatrix}^\top, \quad (3)$$

where $\Delta x_t, \Delta y_t, \Delta \phi_t, \Delta v_t$ represent relative longitude, relative latitude, relative course of the ground (COG), and relative speed of the ground (SOG), respectively. These motion parameters are shown in Fig. 1a.

The relative motions z_t serve to infer the hidden intent of target ship. These observations can be used to express a likelihood function that relates the own ship's motion state s_t^O to the target ship's motion state s_t;

$$p(z_t \mid s_t) = \mathcal{N}(z_t \mid s_t - s_t^O, R), \quad (4)$$

where R is the observation noise of AIS data. Note that s_t^O is observed and is not a random variable. The motion state of target ship is denoted as

$$s_t = \begin{bmatrix} x_t & y_t & \phi_t & v_t \end{bmatrix}^\top, \quad (5)$$

where x_t and y_t represent the longitude and latitude respectively, ϕ_t represents the COG, and v_t represents the SOG.
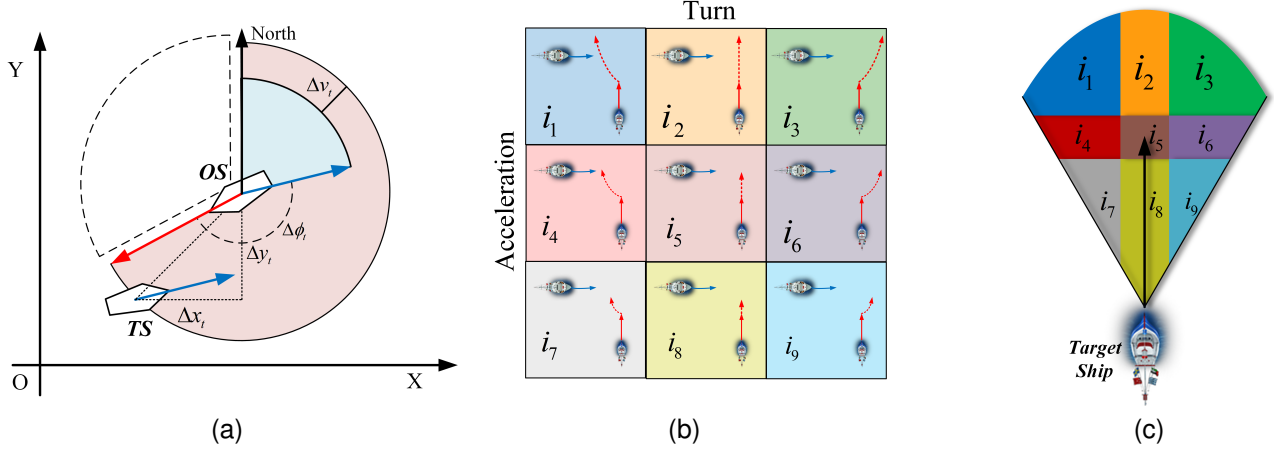
Fig. 1. Avoidance intents during the ship encounter. (a) The observation is the relative motion parameters of two ships, which consist of relative longitude, relative latitude, relative COG, and relative SOG. (b) Multi-class avoidance intents of the target ship. The blue arrows represent the own ship, and the red arrows represent the target ship. The dotted line represents the navigation trend of the target ship. For instance, i_1 represents the target ship intended to turn left and accelerate. (c) The intent consists of the combination of different accelerations and turning rates.
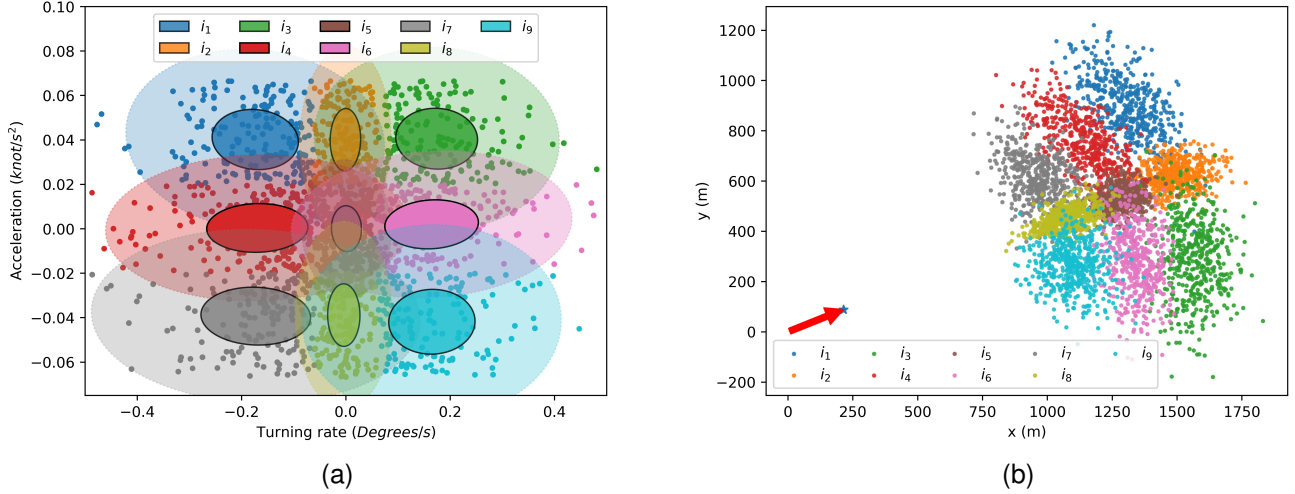

Fig. 2. Avoidance intents of ships (a) Distribution of control signals with different intents in historical AIS data. (b) Simulated future position with different intents (150 seconds later).

C. Ship dynamics

We label the acceleration a_t and turning rate w_t as the control signals u_t:

$$u_t = \begin{bmatrix} w_t & a_t \end{bmatrix}^\top . \quad (6)$$

The control signal changes the motion state of the ship. The motion state transition depends on a function F of the previous state and the control signals, and process noise q_t:

$$s_t = F(s_{t-1}, u_t) + q_t , \quad (7)$$

where $q_t \sim \mathcal{N}(0, Q)$ and the function F is defined in [14], as articulated below:

$$F(s_{t-1}, u_t) = \quad (8)$$

$$\underbrace{\begin{bmatrix} \hat{v}_{t-1} \cdot \sin(\hat{\phi}_{t-1})\Delta t \\ \hat{v}_{t-1} \cdot \cos(\hat{\phi}_{t-1})\Delta t \\ 0 \\ 0 \end{bmatrix}}_{A_t} + \underbrace{\begin{bmatrix} x_{t-1} \\ y_{t-1} \\ \phi_{t-1} \\ v_{t-1} \end{bmatrix}}_{s_{t-1}} + \underbrace{\begin{bmatrix} 0 & 0 \\ 0 & 0 \\ \Delta t & 0 \\ 0 & \Delta t \end{bmatrix}}_{B} \underbrace{\begin{bmatrix} w_t \\ a_t \end{bmatrix}}_{u_t},$$

where Δt is the sampling rate. A_t is constructed from a first-order Taylor approximation of a constant-velocity constant turn-rate motion model with the approximating point at $\hat{s}_{t-1} = \mathbb{E}_{p(s_{t-1} \mid z_{1:t-1})}[p(s_{t-1} \mid z_{1:t-1})]$. Note that the transition matrix A_t is time-varying. The specifics of Eq. 8 are available in the Appendix.

Given Eq. 7-8, the state transition can be written as:

$$p(s_t \mid s_{t-1}, u_t) = \mathcal{N}(s_t \mid F(s_{t-1}, u_t), Q) . \quad (9)$$

The sequence depends on an initial state which may be partially unknown. We define the state prior distribution as

$$p(s_0) = \mathcal{N}(s_0 \mid m_0, \Sigma_0). \tag{10}$$

D. Intent-driven control prior

Our beliefs about appropriate values are characterized by a categorical distribution

$$p(I_t) = \text{Cat}(I_t \mid \pi_t), \tag{11}$$

where Cat represents Categorical distribution and the (time-varying) parameters

$$\pi_t = \{\pi_{tk} : k \in \mathbb{I}, \sum_{k \in \mathbb{I}} \pi_{tk} = 1\} \tag{12}$$

indicate the probability of each intent. We chose the categorical distribution to represent intent due to its suitability for modeling discrete outcomes, aligning with the distinct and predefined nature of different ship intents.

For each intent state, the ship officers change the ship motion state by controlling the propeller and rudder. This operation will generate the power for acceleration and turning of the ship. The control variable is modeled as a noisy realization of the intent class

$$p(u_t \mid I_t = k) = \mathcal{N}(u_t \mid m_k, \Sigma_k), \tag{13}$$

with mean m_k and variance Σ_k. As such, we can write the control variable's dependence on all intent classes as a Gaussian mixture model (GMM)

$$p(u_t \mid I_t) = \prod_{k \in \mathbb{I}} \mathcal{N}(u_t \mid m_k, \Sigma_k)^{[I_t = k]}. \tag{14}$$

GMM is a flexible probabilistic model that combines multiple Gaussian distributions, allowing it to model intricate distributions with various control modes. By employing a GMM in the ship dynamic model, we acknowledge and accommodate the potential existence of distinct patterns in how ship officers control the vessel for different intents. The probabilistic nature of the GMM enables to account for uncertainties and variations in the intent-to-control mapping, and the results are shown in Fig. 2.

V. INFERENCE

A. A factor graph representation of the intent model

With Eq. 2, we get the full probabilistic model. Since we are interested in the posterior of the hidden intent $p(I_t|z_{1:t})$, the other variables should be marginalized. However, the encounter is a long-lasted process, and many factors evolved. The marginalization suffer from the "curse of dimensionality". Factor graphs provide a automatable approach to solving inference problems.

Hence, we represent the probabilistic dynamical model by a Forney-style Factor Graph [32], which is shown in Fig. 3. In the graph, each edge represents a variable and each node represents a factor. A node connected to an edge denotes that the variable is an argument of this factor. See Fig. 4 for two examples. In Fig. 4a, the control signals depend on the intent class, which refers to Eq. 14. Intent class I_t and control signal u_t are the arguments of this node, and the relationship between them is characterized as a GMM. Fig. 4b represents the motion state transition process, which refers to Eq. 7-9. The vertical edges reflect the "intent-control-state-observation" procedure, and the horizontal edges indicate how the encounter situation evolves over time.

The intent inference are executed through a prediction-correction procedure. At $t = 1$, the prediction step consists of applying the Chapman-Kolmogorov integral to the state transition [33, Ch. 4]

$$p(s_1, I_1)$$
$$= \int \underbrace{p(s_1 \mid s_0, u_1)}_{\text{state transition}} \underbrace{p(u_1 \mid I_1)}_{\text{control}} \underbrace{p(I_1)p(s_0)}_{\text{priors}} \mathrm{d}s_0 \mathrm{d}u_1. \tag{15}$$

The update step consists of applying Bayes' rule where the evidence term can be computed by marginalization over all unobserved variables

$$p(z_1) = \sum_{I_1} \int p(z_1, s_1, I_1) \mathrm{d}s_1. \tag{16}$$

At $t = 2$, we repeat the prediction and correction steps but rely on the posterior from $t = 1$ as the prior distribution. However, we only need the state posterior since we assume that intents are fixed over time. Hence,

$$p(s_1 \mid z_1) = \sum_{I_1} p(s_1, I_1 \mid z_1). \tag{17}$$

Next, the prediction step is

$$p(s_2, I_2 \mid z_1)$$
$$= \int p(s_2 \mid s_1, u_2) \, p(u_2 \mid I_2) \, p(s_1 \mid z_1) \mathrm{d}s_1 \mathrm{d}u_2. \tag{18}$$

and the update step is given by

$$p(s_2, I_2 \mid z_{1:2}) = \frac{1}{p(z_2 \mid z_1)} p(z_2 \mid s_2) p(s_2, I_2 \mid z_1), \tag{19}$$

where the evidence term can be computed in a similar fashion as before

$$p(z_2 \mid z_1) = \sum_{I_2} \int p(z_2, s_2, I_2 \mid z_1) \mathrm{d}s_2. \tag{20}$$

To generalize to time t, where $t > 1$, the prediction step is given by

$$p(s_t, I_t \mid z_{t-1})$$
$$= \int p(s_t \mid s_{t-1}, u_t) \, p(u_t \mid I_t) \, p(s_{t-1} \mid z_{t-1}) \mathrm{d}s_{t-1} \mathrm{d}u_t, \tag{21}$$

and the update step by

$$p(s_t, I_t \mid z_{1:t}) = \frac{1}{p(z_t \mid z_{1:t-1})} p(z_t \mid s_t) p(s_t, I_t \mid z_{t-1}), \tag{22}$$

where the evidence term is

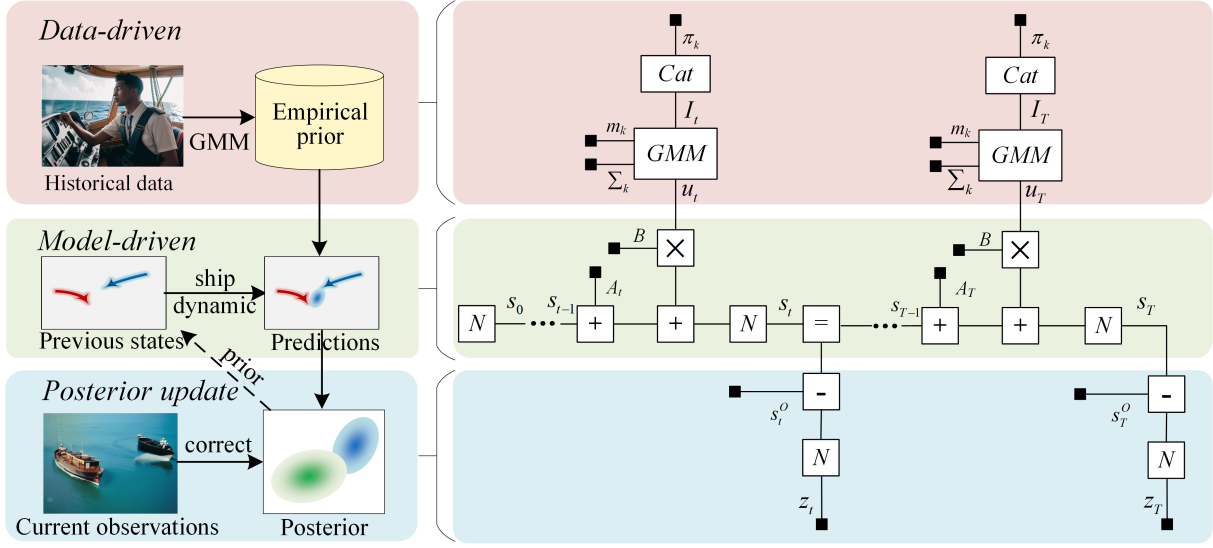$$p(z_t \mid z_{1:t-1}) = \sum_{I_t} \int p(z_t, s_t, I_t \mid z_{1:t-1}) \mathrm{d}s_t. \tag{23}$$

Fig. 3. A Forney-style factor graph representation of the ship intent model in the recursive form, which can be seen in Eq. 2-14. Edges represent variables and nodes represent factors. An edge is connected to a factor if the corresponding variable is an argument to the factor functions. The small black squares denote fixed parameter values and observed variables in the model. The calculation order can be determined based on the given equations. For example, the calculation order for subtraction can be observed in Eq. 4.
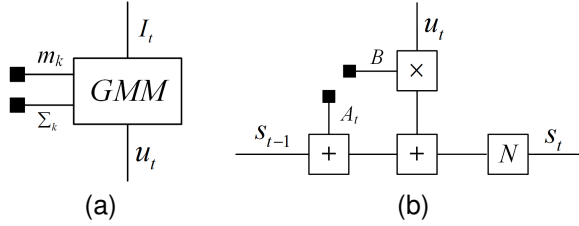

Fig. 4. Sub components of factor graph (a) Control variable depended on intent classes. (b) Motion state transition with time.

B. Message passing on factor graph

In a factor graph, the collective computation described by Eq. 2 can be realized by a series of automated local computations. Each of these local computations plays a role in shaping the intent posterior, and their interaction can be conceptualized as the exchange of messages between nodes within the factor graph. This message passing (MP) is facilitated by the application of the sum-product algorithm [26].

To explain the message passing process, we take a time-segment of the factor graph as an example, as shown in Fig. 5. The arrows represent the message flow in the graph. For instance, the messages on edge I_t are denoted by $\overrightarrow{\mu}(I_t)$ and $\overleftarrow{\mu}(I_t)$, which represent the forward or backward message respectively. The posterior $p(I_t \mid z_{1:t})$ can be obtained by the product of forward and backward messages on the corresponding edge as

$$p(I_t \mid z_{1:t}) = \overrightarrow{\mu}(I_t) \cdot \overleftarrow{\mu}(I_t), \qquad (24)$$

where the forward message is

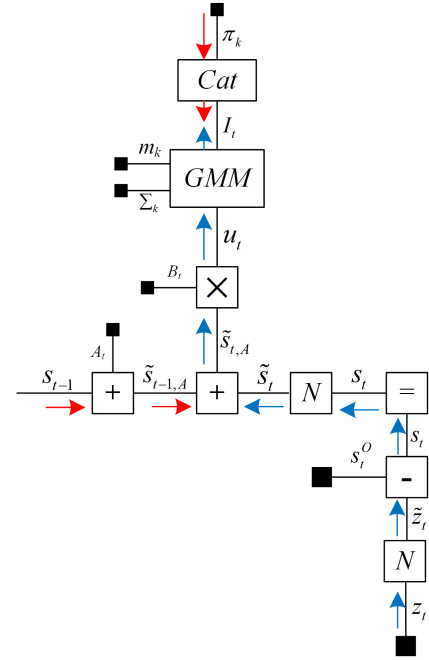$$\overrightarrow{\mu}(I_t) = \text{Cat}(\pi_k), \qquad (25)$$

Fig. 5. Message passing on the factor graph for ship intent inference in one time slice. The red arrows represent the forward messages, and the blue arrows represent the backward messages.

and the backward message is

$$\overleftarrow{\mu}(I_t) = \int \overleftarrow{\mu}(u_t) \prod_{k \in \mathbb{I}} \mathcal{N}(u_t \mid m_k, \Sigma_k)^{[I_t = k]} \mathrm{d}u_t. \qquad (26)$$

The (m_k, Σ_k) are parameters of the GMM, which are obtained by historical AIS data and shown in Fig. 2. Moreover, the message $\overleftarrow{\mu}(u_t)$ refers to the individual control process of the ship.

To explain more clearly, we mark intermediate variables in the factor graph with tildes (see Fig. 5). For example, the intermediate variables between s_t and z_t is marked as $\tilde{z}_t$. Then, the backward message $\overleftarrow{\mu}(u_t)$ is:

$$\overleftarrow{\mu}(u_t) = \int \delta(B\,u_t - \tilde{s}_{t,A})\overleftarrow{\mu}(\tilde{s}_{t,A})\mathrm{d}u_t\,, \quad (27)$$

where $\delta(\cdot)$ is the Dirac delta function. The message from the state $\overleftarrow{\mu}(\tilde{s}_{t,A})$ is

$$\overleftarrow{\mu}(\tilde{s}_{t,A})$$
$$= \int \delta(\tilde{s}_{t,A} + \tilde{s}_{t-1,A} - \tilde{s}_t)\overrightarrow{\mu}(\tilde{s}_{t-1,A})\overleftarrow{\mu}(\tilde{s}_t)\mathrm{d}\tilde{s}_{t,A}\,. \quad (28)$$

It can be seen from Eq. 28 that the message $\overleftarrow{\mu}(\tilde{s}_{t,A})$ combines information from the previous state $\overrightarrow{\mu}(\tilde{s}_{t-1,A})$ and the data $\overleftarrow{\mu}(\tilde{s}_t)$. This demonstrates that information from past beliefs accumulates over time, improving real-time inference.

The message from the previous state consists of

$$\overrightarrow{\mu}(\tilde{s}_{t-1,A}) = \overrightarrow{\mu}(s_{t-1}) + A_t\,. \quad (29)$$

The message from z_t to $\tilde{s}_t$ passes information from the observation to the state and can be computed through

$$\overleftarrow{\mu}(\tilde{z}_t) = \mathcal{N}(\tilde{z}_t \mid z_t, R) \quad (30)$$
$$\overleftarrow{\mu}(s_t) = \mathcal{N}(s_t \mid z_t + s_t^O, R) \quad (31)$$
$$\overleftarrow{\mu}(\tilde{s}_t) = \mathcal{N}(\tilde{s}_t \mid z_t + s_t^O, Q + R)\,. \quad (32)$$

Equations 27-32 are all linear Gaussian operations, with efficient implementations. We will refer to the calculated message $\overleftarrow{\mu}(u_t)$ as

$$\overleftarrow{\mu}(u_t) = \mathcal{N}(u_t \mid m_t^{(u)}, \Sigma_t^{(u)})\,. \quad (33)$$

The posterior of intent I_t can be explained using a specific case

$$p(I_t = k \mid z_{1:t}) = \overrightarrow{\mu}(I_t = k) \cdot \overleftarrow{\mu}(I_t = k)\,, \quad (34)$$

where the rightward prior message is

$$\overrightarrow{\mu}(I_t = k) = \frac{\pi_k}{\sum_{k \in \mathbb{I}} \pi_k}\,, \quad (35)$$

and the leftward likelihood-based message is

$$\overleftarrow{\mu}(I_t = k)$$
$$= \int \overleftarrow{\mu}(\mu_t)\prod_{k \in \mathbb{I}} \mathcal{N}(u_t \mid m_k, \Sigma_k)^{[I_t=k]}\mathrm{d}u_t \quad (36)$$
$$= \int \mathcal{N}(u_t \mid m_t^{(u)}, \Sigma_t^{(u)}) \cdot \mathcal{N}(u_k \mid m_k, \Sigma_k)\mathrm{d}u_t\,. \quad (37)$$

Equation 37 contains a product of two Gaussian distributions, whose solution is explained in [34]. The posterior probability for each intent will be a categorical distribution

$$p(I_t \mid z_{1:t}) = \begin{bmatrix} p(I_t = i_1 \mid z_{1:t}) \\ p(I_t = i_2 \mid z_{1:t}) \\ \vdots \\ p(I_t = i_9 \mid z_{1:t}) \end{bmatrix}\,. \quad (38)$$

Prediction is a matter of finding the most probable intent, i.e., the largest value within this vector.
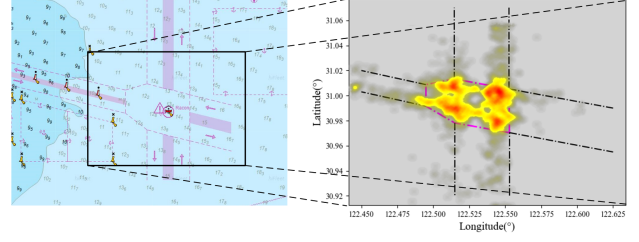

Fig. 6. The study area and the encounter density in the South Channel of Yangtze River Estuary.

VI. Experiment and results

This section discusses the experiments and the inference results in both a quantitative analysis as well as a series of case studies.

TABLE I
CHARACTERISTICS ENCOUNTER DATA SET.

Encounter situation type	Number of ship-pairs	Proportion of type
Head-on	376	8.86%
Overtaking	2899	68.30%
Crossing	969	22.83%

A. Experimental configuration

We conduct experiments on the naturalistic ship encounter data at the South Channel of the Yangtze River Estuary. This waterway covers longitudes $122°450'$–$122°625'$E and latitudes $30°433'$-$31°206'$N. It is busy all year around and is key to the East-China Sea transportation system. There are four channels converging in this area, resulting in many encounters, as shown in Figure 6.

We collected the AIS data in this area and extracted the pairwise trajectories of encounters. The entire data set comprised 4244 encounter scenarios. Among them, 300 scenarios are used for model training and the rest are used for model evaluation. All trajectories are cleaned and synchronized to the same frequency (1/15 Hz), by using the method in [35]. Each time step is labeled as an intent class using the off-line intent calibration method in [36]. This means that after the ship-pairs has completed the encounter, the intent label is assigned to each time step. According to the COLREGs, these encounter scenarios were divided into head-on, overtaking, and crossing. The details of the data are shown in Table I.

The GMM is fitted to the training data set to build what is known as an *empirical prior* distribution [37]. This empirical prior provide the joint distribution of acceleration and turning rate corresponding to the intent, as shown in Fig. 2. The observation noise (R) is configured at 10 m, and the process noise (Q) is set to 1 m.

B. Quantitative analysis

The performance of the proposed model is analyzed using confusion matrices, visualized in Figure 7. It can be seen that the values on the diagonal are large, and that the remaining values are small, especially the ones corresponding to opposite
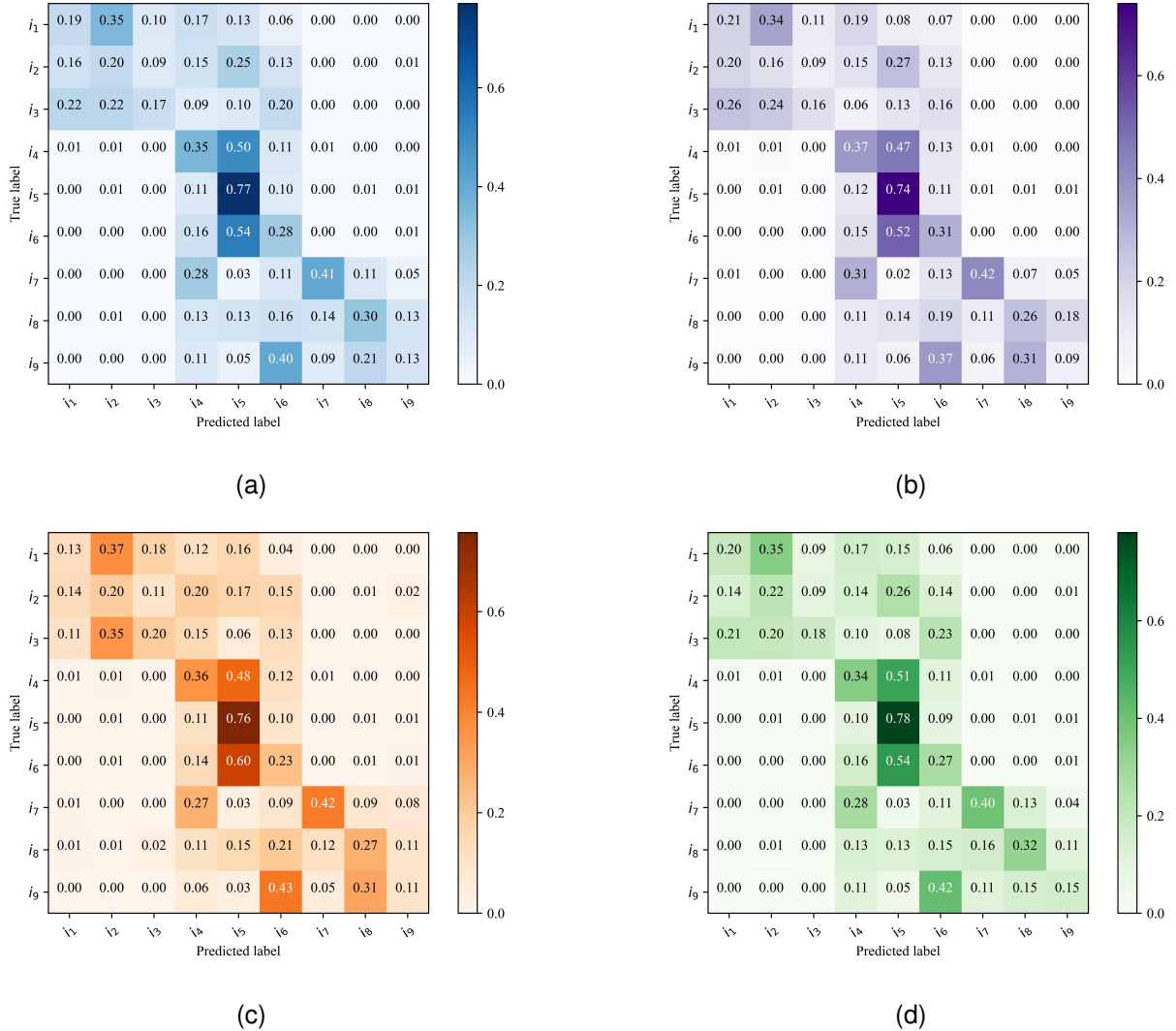
Fig. 7. Confusion matrix of intent inference result. (a) All test set. (b) Crossing situation (c) Head-on situation (d) Overtaking situation. Note that most of the confusion occurs on the first off-diagonals.

classes. For example, the number of samples predicted to be "turn left and decelerate" for a ground truth intent of "turn right and accelerate", is 0. Moreover, as illustrated in the ninth row and sixth column of Fig. 7a, 40% of the samples labeled as "turn right and accelerate" were inferred as "turn right and keep speed." Despite a misjudgment in the speed dimension, the directional information remains valuable, offering ship officers a crucial reference to navigate potential risks.

In addition to accuracy, the lead time of intent inference is extremely important. In Fig. 8, the X-axis is the time when the avoidance intent appears in the ground truth, and the Y-axis is the time when the avoidance intent detected. The points in the red area represent that the intent is predicted in advance, and the points in the blue area represent that the intent is predicted after the ground truth. Note that there are more points in the red area than in the blue area. In general, the intents were predicted in advance, whether from the perspective of the total 9 intent labels or from the perspective of speed and course, respectively. The details of the lead time are shown in Table

II. The average lead time is 0.234 minutes.

Bayesian inference is implemented by using the open-source Julia package `RxInfer` [38][1]. For comparison, we implemented the models in the intent prediction-related studies as the baseline. These baseline models include SVM [7], RF [19], LSTM [20], and ELSTM [9]. For comparison, we implemented the models in the intent prediction-related studies as the baseline. These baseline models include SVM, RF, LSTM, and ELSTM, which are widely used for intent inference in road transportation. The hyperparameters for the models are configured as follows: SVM utilizes an RBF kernel function with a poly degree of 3. For RF, 100 estimators are employed with the Gini criterion. In the case of LSTM, the architecture involves 64 LSTM units, 64 dense neural units, and a learning rate of 0.001. ELSTM is composed of 5 LSTMs, each with identical structure and hyperparameters, employing an ensemble approach to derive the intent classification results.

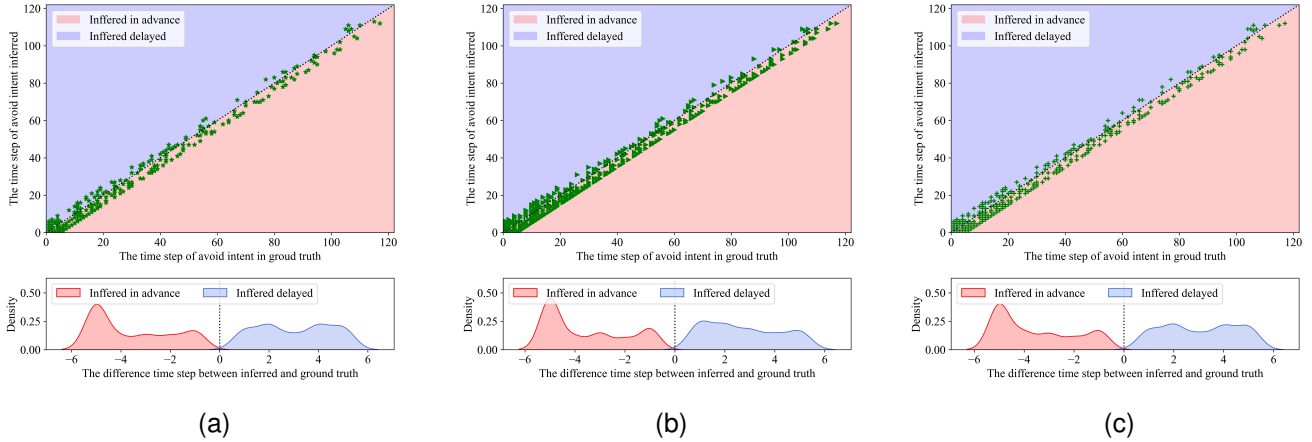[1]https://github.com/biaslab/RxInfer.jl

Fig. 8. Time distribution of intent correctly detected and compared with ground truth. In the upper sub-figure, the samples will fall into the blue (represent the inferred intents are delayed) and red areas (represent the intent are inferred in advance). Note that the number of points in the red area is more than that in the blue area, indicating that intents of most samples can be inferred in advance. The lower sub-figure illustrates the distribution of the difference time step between inferred and ground truth. Note that the difference time equal to 0 is not shown in this lower sub-figure. (a) All 9 avoidance intent classes. (b) Only changing speed. (c) Only changing course

TABLE II
LEAD TIME DISTRIBUTION OF INTENT CORRECTLY DETECTED.

Lead time (minutes)	Crossing		overtaking		head-on		Overall	
Intent type	mean	std	mean	std	mean	std	mean	std
Only changing speed	-0.359	0.175	-0.434	0.187	-0.331	0.178	-0.409	0.184
Only changing course	-0.301	0.205	-0.230	0.190	-0.185	0.207	-0.276	0.202
All 9 avoidance intents	-0.258	0.206	-0.189	0.195	-0.152	0.206	-0.234	0.203

All the code, including additional cases, can be found in this link[2].

We have chosen precision, recall rate, and F1-score as our performance metrics to provide a comprehensive evaluation of the proposed model. Precision (Pr) is calculated as the ratio of true positive count (T_p) to the sum of true positives and false positives (F_p), representing the accuracy of positive predictions. Recall rate (Re) is computed as the ratio of true positive count to the sum of true positives and false negatives (F_n), measuring the model's ability to capture all positive instances. F1-score ($F1$) is derived from precision and recall rate, offering a balanced assessment of the model's overall performance.

The formulas for precision, recall rate, and F1-score are given by:

$$Pr = \frac{T_p}{T_p + F_p} , \ Re = \frac{T_p}{T_p + F_n} , \ F1 = \frac{2(Pr \cdot Re)}{Pr + Re} . \quad (39)$$

These metrics are chosen for their ability to capture both the accuracy and robustness of the model's predictions, providing a well-rounded assessment of its performance.

For the number of total intent classes is 9 and most of them are keeping straight and keep speed, we adopted macro-metrics to evaluate performance. The macro-metrics are computed independently for each intent class and then the average is taken, hence every class, whether it is a majority or minority

[2]https://github.com/biaslab/Chengfeng_intent_inference/

class, is weighted equally. To facilitate a thorough comparison of various methods, we iteratively partitioned the training and testing sets in our experiments. Different training sets were sampled from the entire dataset, and the resulting mean and standard deviation of metrics on the test sets are presented in Table III.

It can be seen from Table III that the proposed Bayesian inference approach outperforms the alternative models on both recall rate and F1-score. For precision, the SVM and RF achieve better performance, but the standard deviation is considerably higher than others. This implies that the SVM and RF algorithms are not as robust for this task as the Bayesian approach.

TABLE III
RESULTS COMPARISON WITH THE BASELINE MODEL.

Algorithms	Precision	Recall	F1-score
SVM	**0.4124** (0.3450)	0.1347 (0.0168)	0.1398 (0.035)
RF	0.3000 (0.1299)	0.17123 (0.0214)	0.1836 (0.032)
LSTM	0.1287 (0.0272)	0.1108 (0.0016)	0.1029 (0.0017)
ELSTM	0.1385 (0.0155)	0.1203 (0.0014)	0.1175 (0.018)
MP	0.2932 (0.0055)	**0.2919** (0.0175)	**0.2843** (0.0092)

C. Case studies

We selected four real encounter situations from the test data set to qualitatively examine the model's performance. Through these case studies, we demonstrate how intent beliefs

TABLE IV
CHARACTERISTICS OF CASES TO EVALUATE INTENT INFERENCE MODEL.

Own ship					Target ship				
MMSI	date	location	SOG	COG	MMSI	date	location	SOG	COG
413408630	2018-12-01	(122.430,31.007)	10.815	102.125	413505980	2018-12-01	(122.517,30.916)	10.398	53.434
		...	...	...			...	...	...
412373480	2018-11-30	(122.433,31.009)	8.297	104.687	413405160	2018-11-30	(122.521,31.045)	7.200	180.060
		...	...	...			...	...	...
413442560	2018-11-30	(122.477,30.998)	10.853	101.556	413918000	2018-11-30	(122.431,31.008)	11.500	103.188
		...	...	...			...	...	...
412350330	2018-11-30	(122.431,31.004)	10.500	104.813	412413848	2018-11-30	(122.537,30.909)	9.900	11.732
		...	...	...			...	...	...

accumulate and propagate, and analyze how intent evolves in specific encounters. The characteristics of these four cases are listed in Table IV.

For case 1, the trajectories of the encountering ships are shown in Fig. 9a. It can be seen that the target ship performs several turns to avoid possible conflicts, even when they are still far apart. This is more clearly present in Fig. 9b, which shows the target ship turning three times, and always keeping speed. The model detects these 15-30 seconds in advance. We use the star and circle to mark the starting and ending point of first avoidance stage. The enlarged drawing in Fig. 9a shows that although the trajectory near the star has no obvious turning, intent can still be correctly detected in advance. Fig. 9c shows the 9 classification probabilities of points ①,②,③ and ④ marked in the Fig. 9b. At point ①, the majority class is "keep speed and course", but there is still a certain probability of keeping speed and turning. At point ②, the intent to turn right was gradually confirmed. That is in line with the avoidance intent growing as the encounter develops, and the officers gradually becoming more convinced. Fig. 9d present the CRI of whole encounter process. It is generally agreed that the bigger the value of DCPA, TCPA and distance the safer the situation will be. The yellow area in Fig. 9d represent the first avoidance stage. Even when the target turned, the situation still became dangerous, and it can be seen by target ship perform two avoidance manoeuvres later on.

Fig. 10 is a typical avoidance operation in a crossing situation. To avoid the own ship, the target ship turned right and passed through the stern of the own ship. This avoidance manoeuvre complies with the requirements of COLREGs. From Fig. 10b we can see that the avoidance intents are inferred before the ground-truth, and Fig. 10c displays the gradual change in intent probabilities. The yellow area in the Fig. 10d suggests that the avoidance manoeuvre occurs when the encountering ships have come very close to each other. Once they sail past each other, the avoidance manoeuvre ends. The DCPA increased in the yellow area, indicating that the risk of conflict was reduced by the avoidance manoeuvre of the target ship.

Fig. 11 displays a complex overtaking situation and the inferred intent at point ① differs from the ground truth. It can be seen from the enlarged drawing in Fig. 11a that the target ship did turn slightly to right. The DCPA (in 11d) increased abruptly in yellow area, which means the target ship performed the avoidance maneuver in time. We speculate that the shift

of direction is too small to be interpreted as avoidance intent.

Fig. 12 display a situation in which two ships form a crossing situation. In the latter stage, the target ship turned right first to avoid the danger. After the conflict situation was resolved, it turned left to resume sailing to the goal direction. At the star point in Fig. 12b, the intent for turning right was detected in advance. Furthermore, at point ③, the intent for turning left was also inferred in advance.

VII. DISCUSSION

The experimental results suggest that the proposed Bayesian model outperforms the set of baseline methods (ref Table. III), and hidden intents can be properly identified in advance (ref Fig.8, Table. II and the case study). While the proposed method exhibits advantages in terms of accuracy and lead-time, it does suffer from the limitations associated with multi-source uncertainties. It can be seen from Fig. 11 and Fig. 12 that the inferred intention changes more frequently than the ground truth. This phenomenon seems to be, at least partly, a consequence of assuming that the noise precision is time-invariant. The ship's motion is perturbed by many external factors, such as wind, waves, oceanic currents and wakes generated by surrounding ships. These factors are not time-invariant, and there may be times when time-invariant noise precision parameters lead to prediction errors. However, this model can still be technically significant in practice for avoiding collisions. Its advantage is that it not only provides the inferred intent label, but also provides a probability for the intentions. The inferred intention with their degrees of confidence can be an important reference for the captain to assess the situation and make avoidance decisions.

VIII. CONCLUSIONS

We proposed a Bayesian modeling approach, with accompanying automatable message passing-based inference on a factor graph, to the problem of intent inference for avoidance of ship collisions. Experimental data was collected in real-world ship encounter scenarios to verify the intent inference model. Quantitative metrics and case studies demonstrate that the developed model is effective in identifying avoidance intents. We have also compared the performance of the proposed model with a set of competitive baseline models, and our method outperformed the alternative methods in most of the metrics. This study holds both theoretical and technical significance in enhancing future ship navigation safety. For
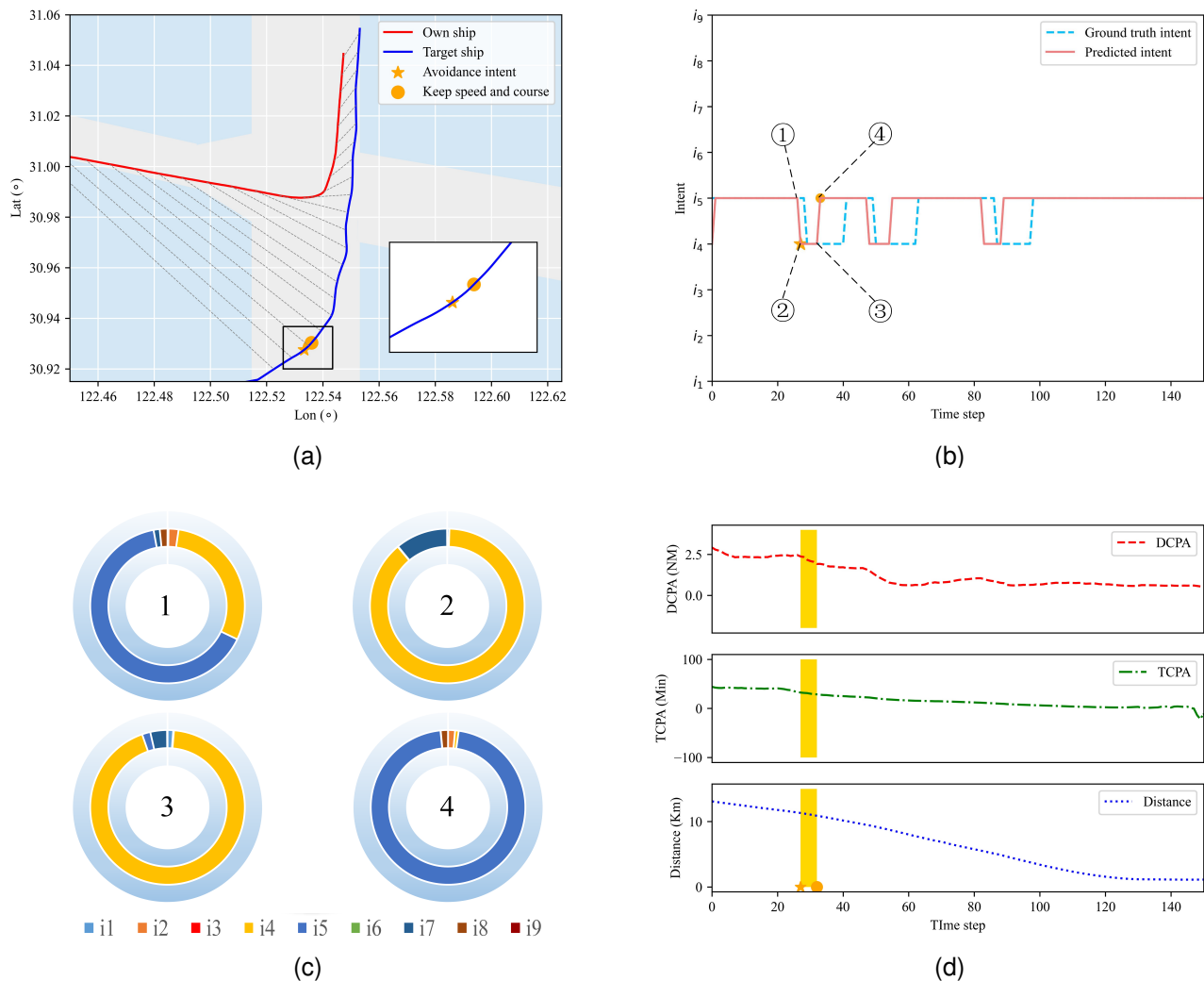
Fig. 9. Case 1. (a) The trajectories of the encountering ships. The grey dotted line connects the position of the two ships at the same time. (b) The inferred intent and the ground truth. It can be seen that the intents are inferred about 2 time steps (30 seconds) in advance. (c) Pie charts of the 9 intent classes, where the length of each color ring represents the probability of the corresponding intent. The number in the ring represents the time point marked in Figure. 9b (d) The DCPA, TCPA and distance of the encountering ships. The yellow area represents the time period for inferred avoidance intent.

instance, when the proposed method infers the avoidance intent of a target ship, the own ship can then either maintain its current direction or turn in the opposite direction, effectively avoiding potential collisions.

For future work, we aim to develop an adaptive noise model to account for possible external disturbances to the ship's motion. In the envisioned future method, automated inference will update the beliefs over the noise's precision parameters, while inferring avoidance intents in real-time. Furthermore, we plan to consider more detailed environmental information, such as electronic chart, wind, wave, and current for the intent inference model, so as to ultimately improve performance.

IX. APPENDIX

The state transition function for ship dynamics (Eq. 8) was proposed by Cho et al. [14]. The undriven component (i.e.,

without Bu_t) is based on the Newtonian dynamics of moving at constant velocity with a constant turn rate:

$$
f(s_{t-1}) = \begin{bmatrix} x_{t-1} + v_{t-1}\sin(\phi_{t-1})\Delta t \\ y_{t-1} + v_{t-1}\cos(\phi_{t-1})\Delta t \\ \phi_{t-1} \\ v_{t-1} \end{bmatrix} \quad (40)
$$

Let $\hat{s}_{t-1}$ be the expected value of the marginal state posterior at time $t-1$, i.e.,

$$
\hat{s}_{t-1} = \mathbb{E}\big[p(s_{t-1} \mid z_{1:t-1})\big]. \quad (41)
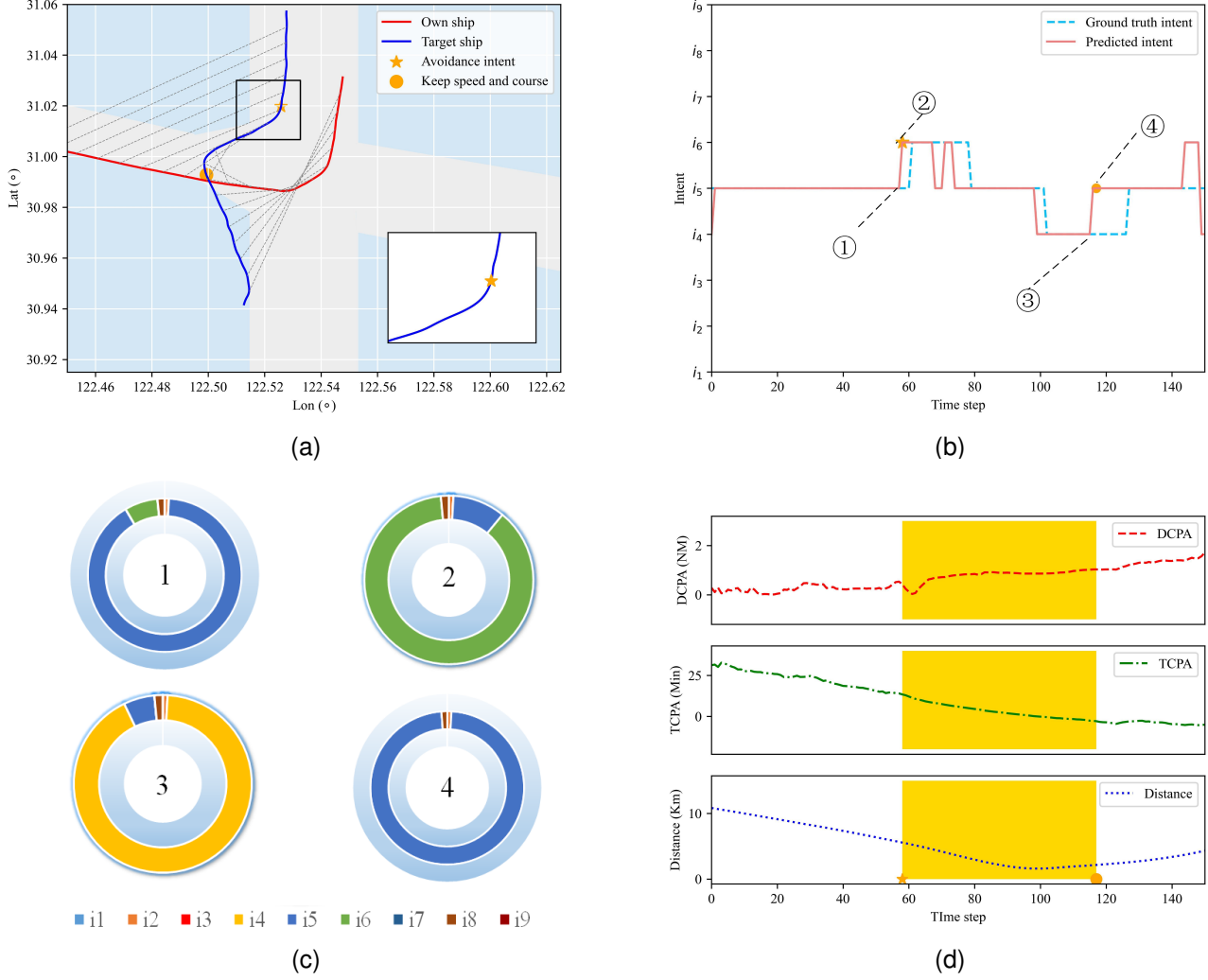$$

(a)

(b)

(c)

(d)

Fig. 10. Case 2. (a) The trajectories of the encountering ships. (b) The inferred intent and the ground truth. It suggests that the intents are inferred about 4 time steps (60 seconds) in advance. (c) Pie charts of the 9 intent classes. (d) The DCPA, TCPA and distance of the encountering ships.

We linearize the nonlinear dynamics using a first-order Taylor approximation evaluated at the point $\hat{s}_{t-1}$:

$$f(s_{t-1}) \approx f(\hat{s}_{t-1}) + J(\hat{s}_{t-1})(s_{t-1} - \hat{s}_{t-1}) \tag{42}$$

$$= \begin{bmatrix} \hat{v}_{t\text{-}1}\sin(\hat{\phi}_{t-1})\Delta t \\ \hat{v}_{t\text{-}1}\cos(\hat{\phi}_{t-1})\Delta t \\ 0 \\ 0 \end{bmatrix} + \begin{bmatrix} x_{t-1} \\ y_{t-1} \\ \phi_{t-1} \\ v_{t-1} \end{bmatrix} + O(s_{t-1}). \tag{43}$$

The first term in Eq. 43 corresponds to our A_t matrix and the second term is the state vector s_{t-1}. The remaining term,

$$O(s_{t-1}, \hat{s}_{t-1}) = \tag{44}$$

$$\begin{bmatrix} \hat{v}_{t\text{-}1}\cos(\hat{\phi}_{t-1})\Delta t(\phi_{t-1}-\hat{\phi}_{t-1})+\hat{v}_{t\text{-}1}\sin(\hat{\phi}_{t-1})\Delta t(v_{t-1}-\hat{v}_{t-1}) \\ -\hat{v}_{t\text{-}1}\sin(\hat{\phi}_{t-1})\Delta t(\phi_{t-1}-\hat{\phi}_{t-1})+\hat{v}_{t\text{-}1}\cos(\hat{\phi}_{t-1})\Delta t(v_{t-1}-\hat{v}_{t-1}) \\ 0 \\ 0 \end{bmatrix}$$

is, in expectation:

$$\mathbb{E}_{p(s_{t\text{-}1}\,\mid\,z_{1:t-1})}\big[O(s_{t\text{-}1}, \hat{s}_{t-1})\big] = 0. \tag{45}$$

During filtering, we take exactly this expectation in the predict step (Eq. 21). So, this remainder term has no effect on the mean of the new state. We therefore ignore this term in the state transition function and work purely with the $A_t + s_{t-1}$ description.

REFERENCES

[1] J. Meng, Y. Liu, R. Bucknall, W. Guo, and Z. Ji, "Anisotropic GPMP2: A fast continuous-time Gaussian processes based motion planner for unmanned surface vehicles in environments with ocean currents," *IEEE Transactions on Automation Science and Engineering*, vol. 19, no. 4, pp. 3914–3931, 2022.

[2] China P&I Club, "Analysis of 108 maritime investigation reports on ship collision accidents," tech. rep., China Ship Owners Mutual Assurance Association, 2020.

[3] China MSA, "Investigation report on the collision accident between the Jiahe 128 and Guiqinyu 22668 ships in the Qiongzhou Strait," tech. rep., 2023.

[4] US Coast Guard, "International regulations for prevention of collisions at sea, 1972 (72 COLREGS)," tech. rep., US Department of Transportation, 1999.
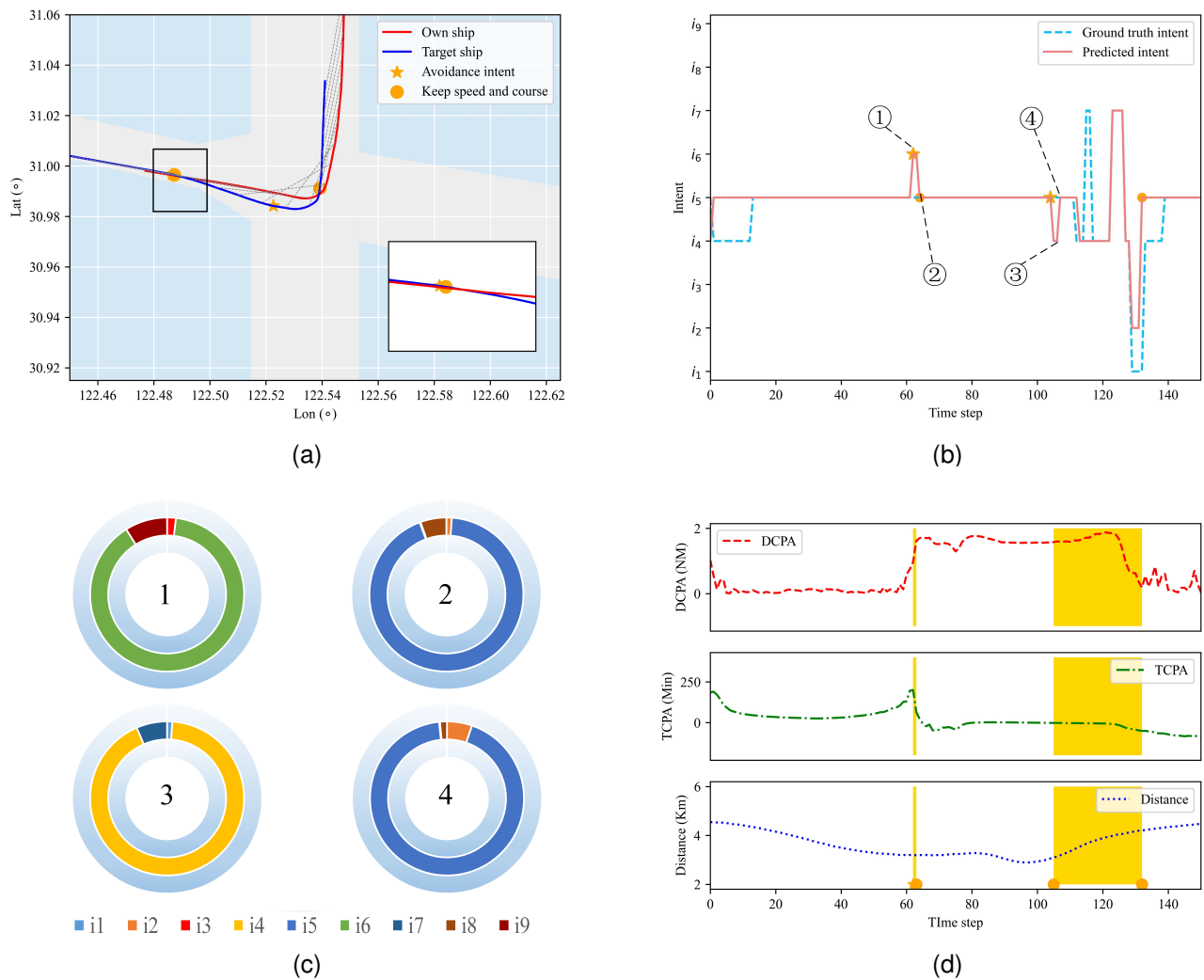
(a)

(b)

(c)

(d)

Fig. 11. Case 3. (a) The trajectories of the encountering ships. (b) The inferred intent and the ground truth. (c) Pie charts of the 9 intent classes. (d) The DCPA, TCPA and distance of the encountering ships.

[5] T. Tengesdal, T. A. Johansen, and E. F. Brekke, "Ship collision avoidance utilizing the cross-entropy method for collision risk assessment," *IEEE Transactions on Intelligent Transportation Systems*, 2021.

[6] J. Ma, C. Jia, X. Yang, X. Cheng, W. Li, and C. Zhang, "A data-driven approach for collision risk early warning in vessel encounter situations using attention-BiLSTM," *IEEE Access*, vol. 8, pp. 188771–188783, 2020.

[7] X. Wang, Y. Guo, C. Bai, Q. Yuan, S. Liu, and J. Han, "Driver's intention identification with the involvement of emotional factors in two-lane roads," *IEEE Transactions on Intelligent Transportation Systems*, vol. 22, no. 11, pp. 6866–6874, 2021.

[8] Y. Wu, C. Chu, F. Chu, and N. Wu, "Heuristic for lane reservation problem in time constrained transportation," in *2009 IEEE International Conference on Automation Science and Engineering*, pp. 543–548, IEEE, 2009.

[9] Y. Xing, C. Lv, H. Wang, D. Cao, and E. Velenis, "An ensemble deep learning approach for driver lane change intention inference," *Transportation Research Part C: Emerging Technologies*, vol. 115, p. 102615, 2020.

[10] H. Rong, A. Teixeira, and C. G. Soares, "Maritime traffic probabilistic prediction based on ship motion pattern extraction," *Reliability Engineering & System Safety*, vol. 217, p. 108061, 2022.

[11] R. Zhen, Z. Shi, J. Liu, and Z. Shao, "A novel arena-based regional collision risk assessment method of multi-ship encounter situation in complex waters," *Ocean Engineering*, vol. 246, p. 110531, 2022.

[12] L. Zhao and X. Fu, "A method for correcting the closest point of approach index during vessel encounters based on dimension data from AIS," *IEEE Transactions on Intelligent Transportation Systems*, vol. 23, no. 8, pp. 13745–13757, 2022.

[13] N. Gu, D. Wang, Z. Peng, and L. Liu, "Observer-based finite-time control for distributed path maneuvering of underactuated unmanned surface vehicles with collision avoidance and connectivity preservation," *IEEE Transactions on Systems, Man, and Cybernetics: Systems*, vol. 51, no. 8, pp. 5105–5115, 2021.

[14] Y. Cho, J. Kim, and J. Kim, "Intent inference of ship collision avoidance behavior under maritime traffic rules," *IEEE Access*, vol. 9, pp. 5598–5608, 2021.

[15] Y. Cho, J. Kim, and J. Kim, "Intent inference-based ship collision avoidance in encounters with rule-violating vessels," *IEEE Robotics and Automation Letters*, vol. 7, no. 1, pp. 518–525, 2022.

[16] T. Wang, Q. Wu, J. Zhang, B. Wu, and Y. Wang, "Autonomous decision-making scheme for multi-ship collision avoidance with iterative observation and inference," *Ocean Engineering*, vol. 197, p. 106873, 2020.

[17] S. Wang, Y. Zhang, and Y. Zheng, "Multi-ship encounter situation adaptive understanding by individual navigation intention inference," *Ocean Engineering*, vol. 237, p. 109612, 2021.

[18] L. Du, F. Goerlandt, O. A. Valdez Banda, Y. Huang, Y. Wen, and P. Kujala, "Improving stand-on ship's situational awareness by estimating the intention of the give-way ship," *Ocean Engineering*, vol. 201, p. 107110,
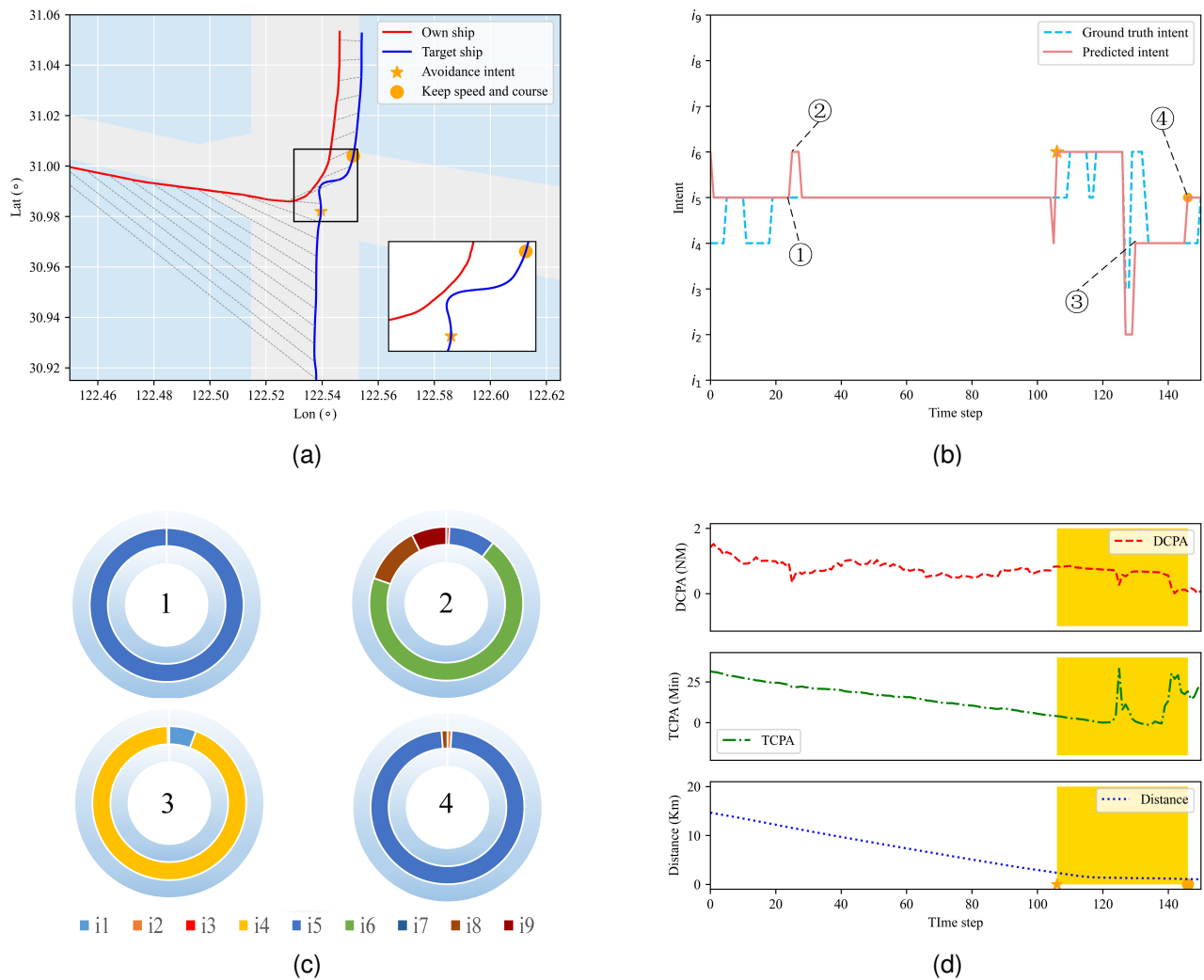
Fig. 12. Case 4. (a) The trajectories of the encountering ships. (b) The inferred intent and the ground truth. (c) Pie charts of the 9 intent classes. (d) The DCPA, TCPA and distance of the encountering ships.

2020.

[19] F. Gross, J. Jordan, F. Weninger, F. Klanner, and B. Schuller, "Route and stopping intent prediction at intersections from car fleet data," *IEEE Transactions on Intelligent Vehicles*, vol. 1, no. 2, pp. 177–186, 2016.

[20] K. Saleh, M. Hossny, and S. Nahavandi, "Intent prediction of pedestrians via motion trajectories using stacked recurrent neural networks," *IEEE Transactions on Intelligent Vehicles*, vol. 3, no. 4, pp. 414–424, 2018.

[21] J. Lee, S. Zhou, and J. Chen, "Robust parameter design on dual stochastic response models with constrained bayesian optimization," *IEEE Transactions on Automation Science and Engineering*, 2023.

[22] E. Skordilis and R. Moghaddass, "A double hybrid state-space model for real-time sensor-driven monitoring of deteriorating systems," *IEEE transactions on automation science and engineering*, vol. 17, no. 1, pp. 72–87, 2019.

[23] F. Garrido-Valenzuela, S. Raveau, and J. C. Herrera, "Bayesian route choice inference to address missed Bluetooth detections," *IEEE Transactions on Intelligent Transportation Systems*, vol. 23, no. 3, pp. 1865–1874, 2022.

[24] R. B. Anderson, C. Pehlivantürk, and M. Pryor, "Optimization strategies for bayesian source localization algorithms," *IEEE Transactions on Automation Science and Engineering*, vol. 20, no. 1, pp. 394–403, 2022.

[25] F. A. N. Palmieri, K. R. Pattipati, G. Fioretti, G. D. Gennaro, and A. Buonanno, "Path planning using probability tensor flows," *IEEE Aerospace and Electronic Systems Magazine*, vol. 36, no. 1, pp. 34–45, 2021.

[26] S. Korl, *A factor graph approach to signal modelling, system identification and filtering*. PhD thesis, ETH Zurich, 2005.

[27] H.-A. Loeliger, J. Dauwels, J. Hu, S. Korl, L. Ping, and F. R. Kschischang, "The factor graph approach to model-based signal processing," *Proceedings of the IEEE*, vol. 95, no. 6, pp. 1295–1322, 2007.

[28] J. Oberländer, S. Klemm, G. Heppner, A. Roennau, and R. Dillmann, "A multi-resolution 3-d environment model for autonomous planetary exploration," in *2014 IEEE International Conference on Automation Science and Engineering (CASE)*, pp. 229–235, 2014.

[29] G. Di Gennaro, A. Buonanno, G. Fioretti, F. Verolla, K. R. Pattipati, and F. A. Palmieri, "Probabilistic inference and dynamic programming: A unified approach to multi-agent autonomous coordination in complex and uncertain environments," *Frontiers in Physics*, vol. 10, p. 944157, 2022.

[30] F. Meyer, P. Braca, P. Willett, and F. Hlawatsch, "A scalable algorithm for tracking an unknown number of targets using multiple sensors," *IEEE Transactions on Signal Processing*, vol. 65, no. 13, pp. 3478–3493, 2017.

[31] B. van Erp, A. Podusenko, T. Ignatenko, and B. de Vries, "A Bayesian modeling approach to situated design of personalized soundscaping algorithms," *Applied Sciences*, vol. 11, no. 20, p. 9535, 2021.

[32] G. D. Forney, "Codes on graphs: Normal realizations," *IEEE Transactions on Information Theory*, vol. 47, no. 2, pp. 520–548, 2001.

[33] S. Särkkä, *Bayesian filtering and smoothing*. No. 3, Cambridge University Press, 2013.

[34] K. Petersen and M. Pedersen, "The matrix cookbook, version 20121115," tech. rep., Technical University Denmark, 2012.

[35] C. Jia, J. Ma, M. He, Y. Su, Y. Zhang, and Q. Yu, "Motion primitives learning of ship-ship interaction patterns in encounter situations," *Ocean Engineering*, vol. 247, p. 110708, 2022.

[36] C. Jia, J. Ma, X. Yang, and X. Lv, "Ragan: A generative adversarial network for risk-aware trajectory prediction in multi-ship encounter situations," *Ocean Engineering*, vol. 289, p. 116188, 2023.

[37] G. Casella, "An introduction to empirical Bayes data analysis," *The American Statistician*, vol. 39, no. 2, pp. 83–87, 1985.

[38] D. Bagaev, A. Podusenko, and B. de Vries, "Rxinfer: A Julia package for reactive real-time Bayesian inference," *Journal of Open Source Software*, vol. 8, no. 84, p. 5161, 2023.
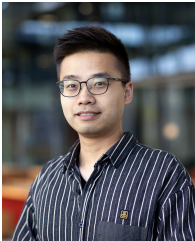
Chengfeng Jia is currently a Ph.D. student in school of navigation, Wuhan university of technology and the guest Ph.D. student in Department of Electrical Engineering, Eindhoven University of Technology. His research interests focus on Bayesian machine learning and intelligent ship Navigation.

Jie Ma received the Ph.D. degree in computer science from the Huazhong University of Science and Technology, Wuhan, China, in 2010. He is currently a Professor with the School of Navigation, Wuhan University of Technology, Wuhan. His researches include networked sensing systems and data-driven intelligent transportation systems, supported by the National Natural Science Foundation of China. He has authored or coauthored over 20 journal and conference papers in the related fields.

Bert de Vries received MSc (1986) and PhD (1991) degrees in Electrical Engineering from Eindhoven University of Technology (TU/e) and the University of Florida, respectively. He is a full professor at the Signal Processing Systems Group at TU/e and directs the BIASlab research team of graduate students with whom he conducts research on transferring a Bayesian brain theory to practical engineering.

Wouter M. Kouw received a MSc (2013) in Neuroscience from Maastricht University, and a PhD (2018) in Computer Science from TU Delft. He was a Niels Stensen Fellow at the University of Copenhagen and is now an assistant professor at TU Eindhoven. His research focuses on neuro-inspired intelligent autonomous systems, implemented as variational Bayesian inference algorithms on probabilistic graphical models.